Spectroscopic investigation of sensitized-Cs ($6^2P_{3/2}$–$6^2P_{1/2}$) laser retrofluorescence in a pure optically thick vapour near a dissipative surface

Karine Le Bris, Claude Kondo Assi, and Jean-Marie Gagné

Abstract: A low-power, monochromatic, tunable diode laser is used to selectively populate the cesium $6^2P_{3/2}$ ($F_e = 2, 3, 4, 5$) hyperfine-structure levels in a pure optically thick vapour in the presence of a dissipative surface. The integrated retrofluorescence intensities for the 852 nm $\left(6^2P_{3/2} \rightarrow 6^2S_{1/2}\right)$, 894 nm $\left(6^2P_{1/2} \rightarrow 6^2S_{1/2}\right)$ and 455 nm $\left(7^2P_{3/2} \rightarrow 6^2S_{1/2}\right)$ lines have been measured and analyzed. When the laser frequency is scanned through the $\left[6^2S_{1/2}\left(F_g\right) \rightarrow 6^2P_{3/2}\left(F_e\right)\right]$ hyperfine resonance line, the sensitized retrofluorescence spectral signal corresponding to the 894 nm line has a profile significantly different from the retrofluorescence signal at the 852 nm line, but rather similar to the profiles of the lines associated with the energy-pooling collisions. The population of the $6^2P_{1/2}$ atomic level in an optically thick vapour cannot be explained only by the fine-structure excitation transfer process $\left[\mathrm{Cs}\left(6^2P_{3/2}\right) + \mathrm{Cs}\left(6^2S_{1/2}\right) \leftrightarrow \mathrm{Cs}\left(6^2P_{1/2}\right) + \mathrm{Cs}\left(6^2S_{1/2}\right)\right]$ usually accepted in an optically thin vapour. We have investigated inelastic collisions in the populating mechanisms of $6^2P_{1/2}$ level starting from the $6^2P_{3/2}$ level exited by the monochromatic laser taking into account the presence of an electrically conductive surface. It appears from our experimental and theoretical investigations that, the spectral properties of the laser-induced Cs 894 nm sensitized retrofluorescence in a pure optically thick vapour near a dissipative surface cannot be explained by both the conventional mechanism and cascade collisions. The satisfactory interpretation of the experimental results is an open problem of atomic spectroscopy.

PACS Nos.: 32.30, 32.50, 32.70, 32.80, 34.10, 34.50, 42.62

Résumé : Une diode-laser monochromatique accordable, de faible puissance, est utilisée pour peupler sélectivement les niveaux de la structure hyperfine $6^2P_{3/2}$ ($F_e = 2, 3, 4, 5$) du Césium dans une vapeur pure, optiquement épaisse et en présence d'une surface dissipative. Les intensités intégrées de rétro-fluorescence des raies 852 nm $\left(6^2P_{3/2} \rightarrow 6^2S_{1/2}\right)$, 894 nm $\left(6^2P_{1/2} \rightarrow 6^2S_{1/2}\right)$ et 455 nm $\left(7^2P_{3/2} \rightarrow 6^2S_{1/2}\right)$ ont été mesurées et analysées. Lorsque le

Received 26 May 2003. Accepted 1 March 2004. Published on the NRC Research Press Web site at http://cjp.nrc.ca/ on 19 May 2004.

K. Le Bris, C. Kondo Assi, and J.-M. Gagné.[1] Laboratoire d'optique et de spectroscopie, Département de génie physique, École Polytechnique de Montréal, C.P. 6079, succursale Centre-Ville, Montréal, QC H3C 3A7, Canada.

[1]Corresponding author (e-mail: jmgagne@polymtl.ca).

laser balaye la raie de résonance hyperfine $\left[6^2S_{1/2}\left(F_g\right) \rightarrow 6^2P_{3/2}\left(F_e\right)\right]$ le signal spectral de rétro-fluorescence sensibilisée correspondant à la raie 894 nm, a un profil différent de celui de la raie 852 nm, et plutôt similaire aux profils des raies associées au processus *energy-pooling collisions*. Le peuplement du niveau atomique $6^2P_{1/2}$ dans une vapeur optiquement épaisse ne peut pas être expliqué uniquement par le processus de transfert d'excitation entre les niveaux fins $\left[\mathrm{Cs}\left(6^2P_{3/2}\right) + \mathrm{Cs}\left(6^2S_{1/2}\right) \leftrightarrow \mathrm{Cs}\left(6^2P_{1/2}\right) + \mathrm{Cs}\left(6^2S_{1/2}\right)\right]$ habituellement admis dans une vapeur optiquement mince. Nous avons étudié des collisions inélastiques comme mécanismes de peuplement du niveau $6^2P_{1/2}$ à partir du niveau $6^2P_{3/2}$ peuplé à l'aide d'un faisceau laser monochromatique en prenant en considération la présence d'une surface conductrice. Il découle de notre étude expérimentale et théorique que ni le mécanisme de collision conventionnel, ni celui de collisions en cascade permet d'interpréter les propriétés spectrales de la rétro-fluorescence sensibilisée induite par laser de la raie Cs 894 nm dans une vapeur pure optiquement épaisse près d'une surface dissipative. L'interprétation satisfaisante des résultats expérimentaux est un problème ouvert de spectroscopie atomique.

1. Introduction

Recently, in refs. 1 and 2, a new laser-induced retrofluorescence spectroscopy (LRS) experiment at a glass – optically thick-Cs-vapour interface was reported. LRS technique consists of measuring the light emitted by excited atoms in the direction opposite to the exciting laser beam (backscattered fluorescence). This technique is efficient for the characterization of atomic processes in an optically thick vapour at the boundary of a dissipative surface. In these works [1, 2], it was shown that surface effects play a key role in atomic excitation transfer at the interface between the glass and the Cs vapour. Near an electrically conductive thin layer adsorbed on a glass surface, at a distance of the order of a wavelength, the atomic evanescent waves (or evanescent photon emission), generated by an atomic dipole, interact strongly with the surface, leading to the loss of the surface excitation energy by a nonradiative channel. This effect is observed without migration of excited atoms and atomic reflection at the surface. When the interval between an excited atom and the surface is a fraction of wavelength, the excited atom has a nonradiative decay rate greater than the spontaneous emission decay. This fact makes the glass – Cs-metal-vapour interface a specific, non-negligible structure in the study of atomic excitation nonradiative transfer.

In a saturated Cs vapour irradiated by a laser beam, where the excited $6^2P_{3/2}$ level is selectively optically pumped, an important retrofluorescence at 894 nm, corresponding to the $6^2P_{1/2} \rightarrow 6^2S_{1/2}$ transition, occurs, in addition to the resonant retrofluorescence 852 nm ($6^2P_{3/2} \rightarrow 6^2S_{1/2}$). This phenomenon is designated here-in as the sensitized retrofluorescence at 894 nm. In the case of an optically thin vapour, the population of the $6^2P_{1/2}$ level is traditionally attributed to the following collisional excitation transfer reaction [3]:

$$\mathrm{Cs}\left(6^2P_{3/2}\right) + \mathrm{Cs}\left(6^2S_{1/2}\right) \leftrightarrow \mathrm{Cs}\left(6^2P_{1/2}\right) + \mathrm{Cs}\left(6^2S_{1/2}\right) \tag{1}$$

In an optically thick vapour (more complex), where energy-pooling collisions occur and where physical effects due to the internal surface of the cell are not negligible, the population of the $6^2P_{1/2}$ level cannot be attributed to only reaction (1). Energy-pooling processes are collisions between excited atoms during which the two atoms pool their internal energy to produce one atom in the ground state and the other one at a highly excited level. In the case of the selective excitation of one level of the atomic 6^2P term, the energy-pooling reaction is of the following form: $\mathrm{Cs}\left(6^2P_J\right) + \mathrm{Cs}\left(6^2P_{J'}\right) \rightarrow \mathrm{Cs}\left(nl_{J''}\right) + \mathrm{Cs}\left(6^2S_{1/2}\right)$, where $nl_{J''}$ is a highly excited level. The $2\mathrm{Cs}\left(6^2P_{3/2}\right)$ energy-pooling collisions have been studied extensively both theoretically and experimentally [4–8]: the more efficient reaction is the one that produces the 6^2D excited state [6].

To our knowledge, no theoretical or experimental spectroscopic works have yet been published describing a thorough study of the population of the $6^2P_{1/2}$ level at the interface between a dissipative

Fig. 1. Schematic of the experimental setup (P, polarization rotator; L, lens; M, mirror; P.P, polarizing prism; P.M, photomultiplier; and D, spatial filter).

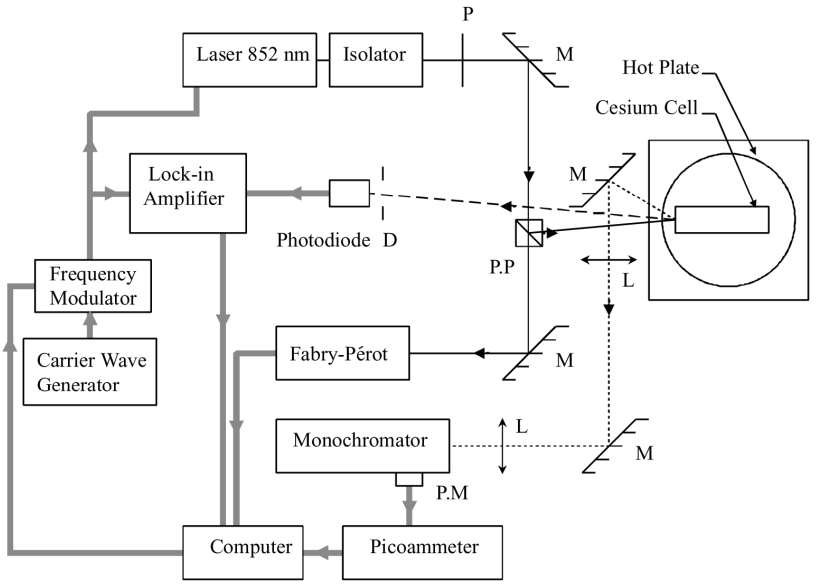

surface and an optically thick Cs vapour, in a regime of selective pumping of $6^2P_{3/2}$. This lack of information motivated us to perform fundamental theoretical and experimental investigations of this spectroscopic problem. The present work is a continuation of the previous ones in refs. 1 and 2. We report, here, new experimental results on the investigation of the populating of the $6^2P_{1/2}$ level when the $6^2P_{3/2}$ level is selectively optically pumped, in the linear regime, with a monochromatic diode laser.

This paper is organized as follows. In Sect. 2, we describe the experimental setup of the laser-induced retrofluorescence spectroscopy. The measurement results are presented in Sect. 3. A brief theoretical analysis and discussion of the possible populating mechanisms of the $6^2P_{1/2}$ level is given in Sect. 4.

2. Retrofluorescence experimental setup

The experimental setup employed in this work is illustrated in Fig. 1. The Cs cell is embedded in an aluminium block and heated to a programmed temperature (between 90 and 180 °C), controlled by a MIRAK thermometer (model HP72935). A diode laser from Environmental Optical Sensors, Inc. (Model LCU 2001), with a bandwidth below 10 MHz, is used to excite the cesium atomic vapour around the 852 nm resonance line. We limited ourselves to weak laser powers (between 20 and 570 μW, for a beam area of $\approx$0.014 cm^2) to avoid nonlinear effects. The calibration is carried out using a Fabry–Pérot interferometer, by directing a fraction of the exciting laser beam to it. The main laser beam is directed to the cylindrical Cs cell along the cell axis, at an angle of incidence of $\approx 2°$ with respect to the normal of the entrance window surface. The fluorescence emitted backward, at an angle of $\approx 16°$ with respect to the normal of the surface, is captured by a Jarell–Ash spectrometer (Model 5) equipped with a photomultiplier. The retrofluorescence signals are amplified by a picoammeter (Keithley Instruments), and are then digitized and recorded by a computer. Frequency-modulated selective-reflection spectroscopy signals are simultaneously collected by a Si photodiode. For studies at high resolution, related to the hyperfine structures of the cesium ground state, covering a bandwidth of 20 GHz, we used a piezo-electric device, having a resolution of a few MHz, to ensure the spectral stepping of the laser sweep.

Fig. 2. Integrated retrofluorescence signal as a function of laser detuning $\Delta\nu_L$ from the resonant 852 nm $\left(6^2S_{1/2} - 6^2P_{3/2}\right)$ line center. The column on the left is for the emission at 852.2 nm, the central column is for 894.3 nm $\left(6^2P_{1/2} \rightarrow 6^2S_{1/2}\right)$, and the column on the right hand side is for emission at the 455 nm $\left(7^2P_{3/2} \rightarrow 6^2S_{1/2}\right)$ line, for various temperatures.

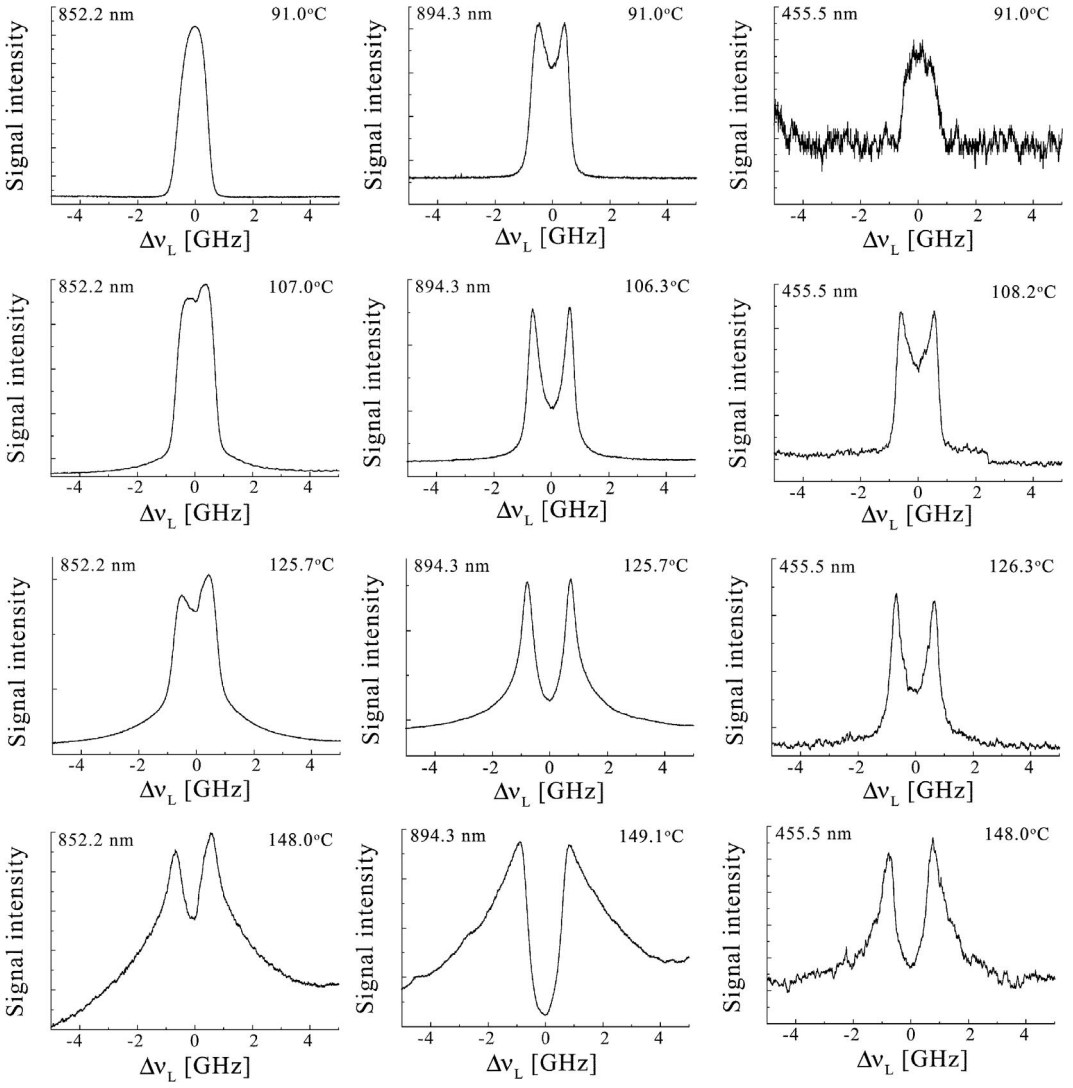

3. Experimental results

The retrofluorescence signals were recorded as a function of laser detuning $\Delta\nu_L$ from the $6^2S_{1/2} - 6^2P_{3/2}$ line center. Figure 2 shows the measurements of the signals emitted at 852, 894, and 455 nm at temperatures of 91, 107, 126, and 148 °C. The profiles correspond to the case of selective pumping, coupling the laser radiation with the particular $6^2S_{1/2}(F_g = 4)$ ground hyperfine structure level.

At 91 °C, the signal at 894 nm exhibits a dip (a minimum centered at zero detuning and two maxima at $\Delta\nu_L \neq 0$) while the signals at 852 and 455 nm do not. Beyond 100 °C, all three signals (at 852, 894, and 455 nm) have an inhibition dip situated at the center. The depth of the dip becomes more prominent when the temperature (and, thus, the density of atoms) of the cell is increased; the dipping is more pronounced for the 894 and 455 nm lines than for the 852 nm line at a given temperature. The

Fig. 3. Experimental ratio η_{exp} between the 894 and 852 nm retrofluorescence intensities as a function of laser detuning, at $T \approx 107$ °C.

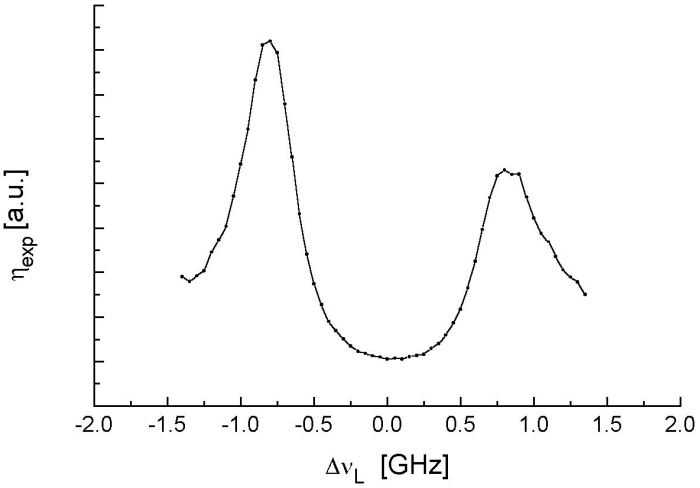

894 and 455 nm profiles have numerous similarities: the two peaks of the signals at 894 and 455 nm are narrower than the peaks of the signal at 852 nm; moreover the peaks of the two lines (894 and 455 nm) are symmetric (i.e., the maxima of the two peaks have the same magnitude) while those of the 852 nm line are asymmetric. The profile of the dip of the signal at 894 nm is similar to the one at 455 nm; however, the signal at 894 nm has an inhibition a little deeper at the center.

At 148 °C, we note that the signal at the line center for 894 nm is lower than the magnitude of the signal at the wings of the profile while, for the 852 and 455 nm lines, the signal at the center still remains higher compared with the signal at the wings. We also note an enlargement of the signal base and an intensity increase at the wings of the integrated retrofluorescence profiles, which is more apparent at 852 and 894 nm than at 455 nm. We have not identified the origin of this behaviour. This could be due to a modification of the properties of the optical filter at the glass–vapour interface. The behaviour of the profiles, at 148 °C (and higher), strongly suggests that, in this temperature range, some more complex processes occur, which have not been investigated here.

Figure 3 shows the experimental integrated retrofluorescent signal ratio $\eta_{exp} = \phi_{894}/\phi_{852}$ corresponding to the optical pumping excitation $6^2S_{1/2}\left(F_g = 4\right) - 6^2P_{3/2}$ ($F_e = 3, 4, 5$), as a function of the laser frequency, at $T = 107$ °C (F_e and F_g being the hyperfine structure quantum numbers). The value of the ratio η_{exp} is strongly distorted into the absorption band of the line. From the experimental retrofluorescent spectral signal in optically thick vapour near a dissipative surface, an elaborate correction is required for the determination of the true collision cross section $Q\left(6^2P_{3/2} - 6^2P_{1/2}\right)$, contrary to the case of optically thin vapour. As mentioned in ref. 1, the trapping of the resonance radiation may not play a dominant role in our experimental results.

4. Theoretical analysis and discussion of the populating mechanisms of the Cs ($6^2P_{1/2}$) level

4.1. Description of the geometry and the physical processes at the glass-window – Cs-vapour interface

In this subsection, we briefly describe the geometrical and physical properties of the interface between the glass and the optically thick saturated Cs vapour irradiated with a laser; we recall the description of the cell-window – vapour interface as developed in ref. 1, to this end, see Fig. 4.

The interface is composed of the internal surface of the glass cell window covered by adsorbates and a slow penetration of Cs atoms into the glass surface underneath, thus forming a thin boundary

Fig. 4. Retrofluorescence cell irradiated by a laser beam: geometrical and physical model of the interface between the glass and the vapour. (*a*) Glass surface with adsorbed Cs atoms (and a low implantation of atoms into the surface underneath); (*b*) the region of the cell where the Cs atoms interact strongly with the glass surface (near-field region); and (*c*) the region where the Cs atoms interact weakly (or not at all) with the glass surface thin metallic film (far-field region).

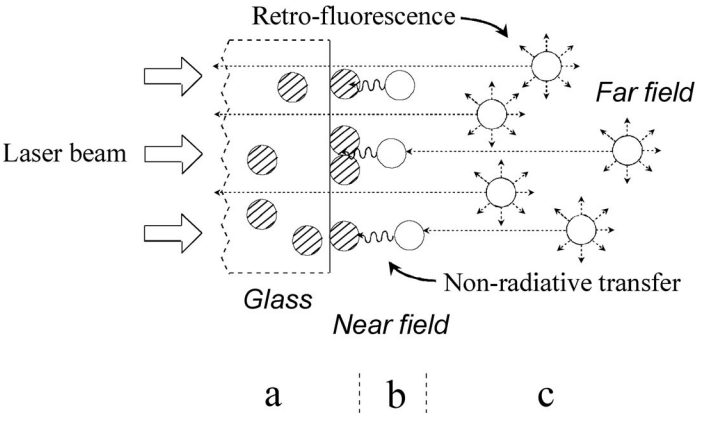

dissipative layer (*a*). Between this metallic layer structure and the Cs vapour reservoir, we consider a so-called near-field region (*b*) or vapour boundary layer. In this wavelength thickness layer, the excited-atomic-states' evanescent waves are highly coupled with the metallic surface [9] leading to a nonradiative loss of the internal energy of the excited atoms. This near-field region contains a large number of atoms in the ground state (7.72×10^{13} at cm^{-3} at 130 °C), uniformly distributed in the volume. The surface and the atoms located in the near-field region constitute a frequency dissipative environment with maximum dissipation situated at the center of the resonance lines. This arrangement is described as a frequency-dissipative optical filter, which partially stops the frequencies contained in a bandwidth centered on the resonance lines. We suppose that each photon (of the laser or of a spontaneous emission of an excited atom) absorbed by an atom located in this region is transformed into thermal energy. Adjacent to the near-field structure is a region of infinite extension containing free atoms that we designate as the far-field region (*c*). In this region, the excited atoms do not (or very weakly) interact with the thin metallic surface. It is particularly in this region that the physical processes that produce the generation of retrofluorescence lines and collisional excitation transfers are important. The far-field region thus becomes a source of light, observable through the window of the cell, propagating in the opposite direction with respect to the laser beam. The cesium vapour reservoir also assumes the role of a thermostat, particularly for the population of hyperfine levels of the ground state.

When the laser is tuned to the 852.2 nm absorption line, we must consider three entrance channels for the energy-pooling collision process: $6^2P_{3/2} + 6^2P_{3/2}$, $6^2P_{3/2} + 6^2P_{1/2}$, and $6^2P_{1/2} + 6^2P_{1/2}$, because the two levels coexist in the vapour. Figure 5 shows a schematic diagram of the most important energy levels of Cs involved in the 2Cs($6^2P_{3/2}$) energy-pooling collisions. The horizontal broken line represents a virtual level located at twice the energy of the $6^2P_{3/2}$ level; the upward dotted arrows ($8^2S_{1/2}$, $4^2F_{5/2,7/2}$) represent endothermic reactions while the downward dotted arrows correspond to exothermic collisions ($7^2P_{1/2,3/2}$, $6^2D_{3/2,5/2}$); the downward straight arrows indicate radiative transitions from the excited levels. Wavelengths are indicated in nanometres. The work of Jabbour et al. [6] indicates that, in Cs vapour resonantly excited at $6^2P_{3/2}$, 6^2D the excited state is predominantly produced during the energy-pooling process (the cross section is at least 10 times larger than the other processes). The reaction $6^2P + 6^2P \rightarrow 6^2D + 6^2S$ in a Cs vapour has been extensively investigated both theoretically and experimentally [4–7]. The investigation of the $6^2P_{3/2}$ and $7^2P_{1/2,3/2}$ levels by retrofluorescence spectroscopy was considered in previous papers [1, 2].

To obtain a quantitative representation of the population of the $6^2P_{1/2}$ level, a number of cascade

Fig. 5. Diagram of energy levels of cesium. The horizontal broken line is located at twice the value of the excited $6^2P_{3/2}$ level energy. The populations of 8^2S, 7^2P, 6^2D, and 4^2F levels are produced by energy-pooling collisions ($6^2P_{3/2} + 6^2P_{3/2}$). The upward bold arrow represents the laser excitation of the $6^2P_{3/2}$ state. The downward straight arrows represents radiative transitions and the dotted arrows are collisional processes. The wavelengths of the transitions are given in nanometres.

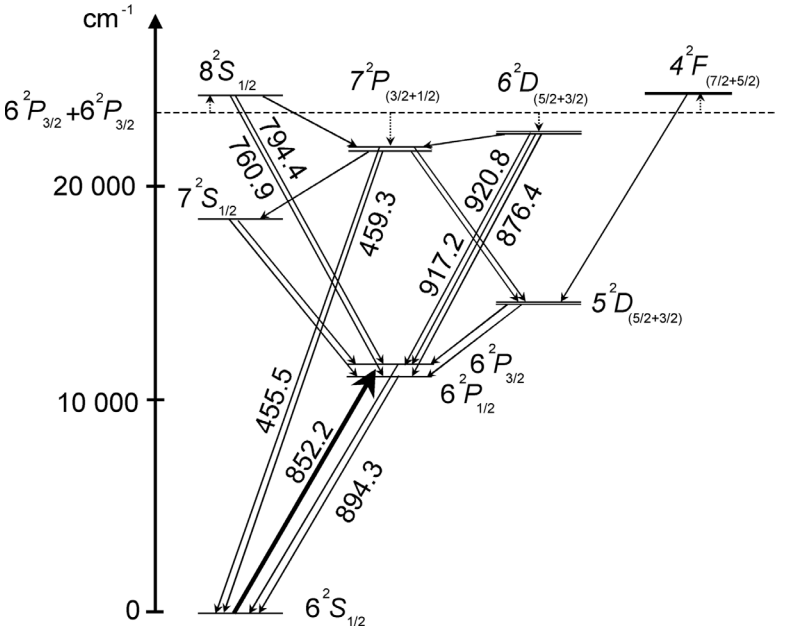

processes must be considered. Besides reaction (1) possibly observable in the vapour, the $6^2D + 6^2S \rightarrow 6^2P + 6^2P$ inverse reaction of the energy-pooling collision has been reported by Yabuzaki et al. [10], using an approach different from ours. This reaction populates the two fine-structure levels $6^2P_{1/2}$ and $6^2P_{3/2}$ in an optically thick vapour. We consider the following reaction:

$$\mathrm{Cs}\left(6^2P_{3/2}\right) + \mathrm{Cs}\left(6^2P_{3/2}\right) \rightarrow \mathrm{Cs}\left(6^2D\right) + \mathrm{Cs}\left(6^2S_{1/2}\right) \rightarrow \mathrm{Cs}\left(6^2P_{3/2,1/2}\right) + \mathrm{Cs}\left(6^2P_{1/2}\right) \qquad (2)$$

as one possible reaction in the populating of the $6^2P_{1/2}$ level.

In focusing our attention on reactions (1) and (2), we can neglect a number of energy levels and transitions in Fig. 5. Figure 6 schematically represents the energy levels and processes that we retain for interpreting the population of the $6^2P_{1/2}$ level. The atomic terms are composed of two hyperfine $\mathrm{Cs}\left(6^2S_{1/2},\ F_\mathrm{g} = 3 \text{ or } 4\right)$ ground levels energetically separated by a gap of 9.192 GHz and four hyperfine $\mathrm{Cs}\left(6^2P_{3/2},\ F_\mathrm{e} = 2, 3, 4, \text{ and } 5\right)$ excited levels covering an interval of 604 MHz. We can consider, in our case, that the two levels, $F_\mathrm{g} = 3$ and 4, are energetically sufficiently separated to ensure that the laser is coupled with only one particular hyperfine level F_g of the ground state. In considering both collisions and kinetic-energy distribution in the saturated vapour, it is reasonable in the first approximation to suppose that a complete redistribution of the population of the excited state occurs in our case. The intensity of the laser beam is sufficiently weak to ensure that the number of excited atoms remains much less than the number of atoms in the ground level. In this case, the population density of atoms in the ground state is considered practically constant and uniform throughout the volume of the cell. The radiative transitions in the far-field region are represented by downward straight arrows in Fig. 6; $\Gamma^{\mathrm{eff}}_{6^2D\rightarrow 6^2P_J}$ is the effective radiative rate for the $6^2D \rightarrow 6^2P_J$ transition, and $\Gamma^{\mathrm{eff}}_{6^2P_J\rightarrow 6^2S_{1/2}}$ is the effective radiative rate for the $6^2P_J \rightarrow 6^2S_{1/2}$ transition. The broken arrows represent collisional processes in the far-field region; $k^{(3/2)}_{6^2D}$ is the energy-pooling coefficient for the 6^2D levels, $k'_{6^2D\rightarrow 6^2P_J}$

Fig. 6. Schematic representation of the energy levels and the mechanisms involved in the populating of the $6^2P_{1/2}$ level. F_g and F_e are the hyperfine structure quantum numbers of the ground and excited state, respectively. Collisional processes are represented by broken arrows and radiative processes by downward continuous arrows. The $6^2P_{3/2}$ level is selectively populated by laser (bold upward arrow coupling $6^2S_{1/2}$ (F_g) to $6^2P_{3/2}$ (F_e)). The 6^2D levels are produced by $6^2P_{3/2} + 6^2P_{3/2}$ energy-pooling collision. The mechanisms in competition in the populating of $6^2P_{1/2}$ level are (*i*) collision $6^2P_{3/2} + 6^2S_{1/2} \rightarrow 6^2P_{1/2} + 6^2S_{1/2}$ and (*ii*) the populating channel starting from 6^2D levels.

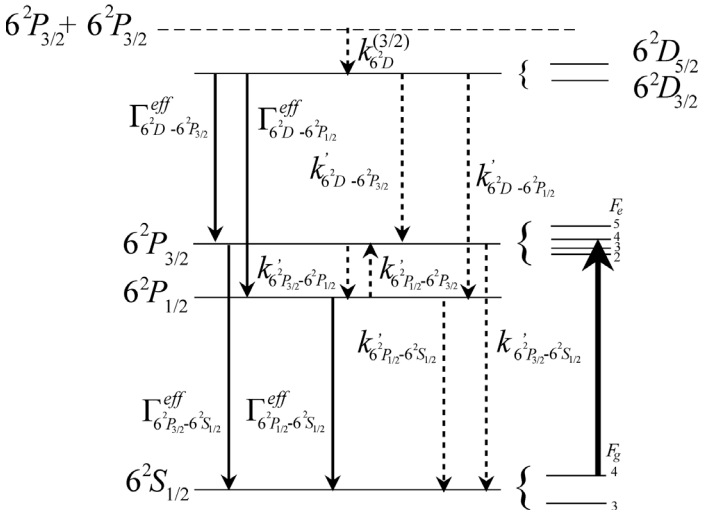

is the collisional rate between the 6^2D state and the ground state for the production of 6^2P atoms. $k'_{6^2P_J \rightarrow 6^2P_{J'}}$ designates the fine-structure changing rate, and $k'_{6^2P_J \rightarrow 6^2S_{1/2}}$ is the collisional quenching decay rate for the 6^2P_J levels. The $\mathrm{Cs}(6^2P_{3/2})$ atomic level is selectively excited by diode laser. The 6^2D levels are essentially populated by $2\mathrm{Cs}(6^2P_{3/2})$ energy-pooling collisions. The relaxation of the 6^2D levels populates the $6^2P_{1/2}$ level (either by the radiative channel or by collision with atoms in the ground state). Our schematization of the atomic levels is reasonable, when we limit ourselves to the consideration of the populating mechanisms of the $6^2P_{1/2}$ level.

On the basis of the physical description given in this subsection, we will discuss, in Subsect. 4.2, the possible dominant mechanisms of $6^2P_{1/2}$ populating, by exploiting the experimental measurement results of LRS.

4.2. Populating mechanisms of the Cs ($6^2P_{1/2}$) level

Here, we discuss two possible mechanisms for the $6^2P_{1/2}$ population in the cell. For each one of the possible mechanisms considered, we give the theoretical formulation of the retrofluorescence integrated signal associated with 894 nm $(6^2P_{1/2} \rightarrow 6^2S_{1/2})$, which is compared with experiment. We employed the same mathematical formalism that has been successfully used for the 852 and 455 nm lines, obtained under the same experimental conditions, to investigate the case of the 894 nm line. Details of the modelling of the 852 and 455 nm retrofluorescence line are given, respectively, in refs. 1 and 2. Two important characteristic aspects of retrofluorescence spectra must be taken into account when dealing with retrofluorescence signals for atomic process investigation: the retrofluorescence intensity dependence on laser power and the sensitized laser retrofluorescence line shapes. A model of the atomic excitation transfer mechanism in vapour is acceptable if the theoretical fluorescence signal (derived from the transfer mechanism) is compatible with both characteristic aspects of the experimental spectra. We take these two aspects into account here when discussing the different possible mechanisms of $6^2P_{1/2}$ populating the cell.

4.2.1. Mechanism (1): collisions Cs ($6^2\mathbf{P_{3/2}}$) + Cs ($6^2\mathbf{S_{1/2}}$) → Cs ($6^2\mathbf{P_{1/2}}$) + Cs ($6^2\mathbf{S_{1/2}}$)

Reaction (1) is usually admitted to explain the population of the $6^2P_{1/2}$ level in a thin cesium vapour selectively optically pumped in $6^2P_{3/2}$. If we consider (1) as dominant in our case, then, neglecting the depopulation of $6^2P_{1/2}$ level due to the migration of excited atoms and assuming a full thermalization of the excited level, the population density of the $6^2P_{1/2}$ level should be given by the following rate equation:

$$\begin{aligned}\frac{\mathrm{d}n_{6^2P_{1/2}}(x,\nu_\mathrm{L},F_\mathrm{g})}{\mathrm{d}t} &= k'_{6^2P_{3/2}\to 6^2P_{1/2}} n_{6^2S_{1/2}} n_{6^2P_{3/2}}(x,\nu_\mathrm{L},F_\mathrm{g}) \\ &- k'_{6^2P_{1/2}\to 6^2P_{3/2}} n_{6^2S_{1/2}} n_{6^2P_{1/2}}(x,\nu_\mathrm{L},F_\mathrm{g}) \\ &- k'_{6^2P_{1/2}\to 6^2S_{1/2}} n_{6^2S_{1/2}} n_{6^2P_{1/2}}(x,\nu_\mathrm{L},F_\mathrm{g}) \\ &- \Gamma^{\mathrm{eff}}_{6^2P_{1/2}\to 6^2S_{1/2}} n_{6^2P_{1/2}}(x,\nu_\mathrm{L},F_\mathrm{g}) \end{aligned} \tag{3}$$

where $n_{6^2P_{1/2}}(x,\nu_\mathrm{L},F_\mathrm{g})$, $n_{6^2P_{3/2}}(x,\nu_\mathrm{L},F_\mathrm{g})$, and $n_{6^2S_{1/2}}$ are, respectively, the population densities of the $6^2P_{1/2}$, $6^2P_{3/2}$, and $6^2S_{1/2}$ levels at a distance x from the internal surface of the cell window, for an excitation laser frequency ν_L, when the atoms are pumped from the particular ground hyperfine level F_g. In the stationary regime, we have

$$n_{6^2P_{1/2}}(x,\nu_\mathrm{L},F_\mathrm{g}) = \frac{k'_{6^2P_{3/2}\to 6^2P_{1/2}}}{k'_{6^2P_{1/2}\to 6^2P_{3/2}} + k'_{6^2P_{1/2}\to 6^2S_{1/2}} + \frac{\Gamma^{\mathrm{eff}}_{6^2P_{1/2}\to 6^2S_{1/2}}}{n_{6^2S_{1/2}}}} \times n_{6^2P_{3/2}}(x,\nu_\mathrm{L},F_\mathrm{g}) \tag{4}$$

Details of the expression of the population density of the $6^2P_{3/2}$ level are given in ref. 2. Note that from this interpretation, $n_{6^2P_{1/2}}(x,\nu_\mathrm{L},F_\mathrm{g})$ and $n_{6^2P_{3/2}}(x,\nu_\mathrm{L},F_\mathrm{g})$ are linearly related. According to this viewpoint, and neglecting radiation-trapping effects in the vapour, the simplified forms of the normalized retrofluorescence signals for the 852, 894, and 455 nm lines are given for qualitative illustration and comparison

$$\phi_{852}(\nu_\mathrm{L},F_\mathrm{g}) \propto F_{\nu_\mathrm{L}} \frac{1}{K_0 + \bar{k}^l_\mathrm{T}(\nu_\mathrm{L})} \bar{k}^l_\mathrm{T}(\nu_\mathrm{L}) \exp\left[-\bar{\tau}^f_\mathrm{T}(\nu_\mathrm{L})\right] \tag{5}$$

$$\phi_{894}(\nu_\mathrm{L},F_\mathrm{g}) \propto F_{\nu_\mathrm{L}} \frac{1}{K'_0 + \bar{k}^l_\mathrm{T}(\nu_\mathrm{L})} \bar{k}^l_\mathrm{T}(\nu_\mathrm{L}) \exp\left[-\bar{\tau}^f_\mathrm{T}(\nu_\mathrm{L})\right] \tag{6}$$

$$\phi_{455}(\nu_\mathrm{L},F_\mathrm{g}) \propto F^2_{\nu_\mathrm{L}} \bar{k}^l_\mathrm{T}(\nu_\mathrm{L}) \exp\left[-2\bar{\tau}^f_\mathrm{T}(\nu_\mathrm{L})\right] \tag{7}$$

where F_{ν_L} is the intensity of the laser beam at the cell entrance window, $\bar{k}^l_\mathrm{T}(\nu_\mathrm{L})$ and $\bar{\tau}^f_\mathrm{T}(\nu_\mathrm{L})$ are, respectively, the total effective spectral absorption coefficient of the saturated vapour located in the far-field region, and the total effective optical thickness of the stop-band filter summed over all the sublevels transitions $|F_\mathrm{g}=4\rangle \to |F_\mathrm{e}=5,4,3\rangle$, and K_0 and K'_0 are constants. The coefficients $\bar{k}^l_\mathrm{T}(\nu_\mathrm{L})$ and $\bar{\tau}^f_\mathrm{T}(\nu_\mathrm{L})$ are related to the atomic parameters given by Le Bris et al. in ref. 1

$$\bar{k}^l_\mathrm{T}(\nu_\mathrm{L}) = \frac{\lambda^2}{8\pi}\frac{2J_\mathrm{e}+1}{2J_\mathrm{g}+1} A_{J_\mathrm{e}\to J_\mathrm{g}} \bar{n}_{F_\mathrm{g}} \sum_{F_\mathrm{e}} g_{F_\mathrm{e}F_\mathrm{g}} \alpha^l_{F_\mathrm{g}\to F_\mathrm{e}}(\nu_\mathrm{L}) \tag{8}$$

$$\bar{\tau}_{\mathrm{T}}^{f}(\nu_{\mathrm{L}}) = \frac{\lambda^2}{8\pi}\frac{2J_{\mathrm{e}}+1}{2J_{\mathrm{g}}+1}\,\bar{A}^{f}_{J_{\mathrm{e}}\to J_{\mathrm{g}}}\bar{n}_{F_{\mathrm{g}}}\,\bar{x}_f\sum_{F_{\mathrm{e}}} g_{F_{\mathrm{e}}F_{\mathrm{g}}}\,\alpha^{f}_{F_{\mathrm{g}}\to F_{\mathrm{e}}}(\nu_{\mathrm{L}}) \tag{9}$$

$$g_{F_{\mathrm{e}}F_{\mathrm{g}}} = \frac{(2F_{\mathrm{e}}+1)\left(2F_{\mathrm{g}}+1\right)}{(2I+1)}\{\ldots 6j\ldots\}^2 \tag{10}$$

where $\bar{n}_{F_{\mathrm{g}}}$ is the mean number density of the ground hyperfine level $\left|F_{\mathrm{g}}\right\rangle$, a well-known function of temperature T, $\alpha^{l}_{F_{\mathrm{g}}\to F_{\mathrm{e}}}(\nu_{\mathrm{L}})$ and $\alpha^{f}_{F_{\mathrm{g}}\to F_{\mathrm{e}}}(\nu_{\mathrm{L}})$ are, respectively, the normalized absorption profile in the far-field region, and in the near-field region for each hyperfine line $6^2S_{1/2}\left(F_{\mathrm{g}}\right) \to 6^2P_{3/2}\left(F_{\mathrm{e}}\right)$, $A_{J_{\mathrm{e}}\to J_{\mathrm{g}}}$ is the Einstein coefficient for spontaneous emission between the two degenerate levels $6^2P_{3/2}$ and $6^2S_{1/2}$ whose statistical weights are $(2J_{\mathrm{e}}+1)$ and $(2J_{\mathrm{g}}+1)$, respectively, $\bar{A}^{f}_{J_{\mathrm{e}}\to J_{\mathrm{g}}}$ is the effective $\left(6^2P_{3/2}\to 6^2S_{1/2}\right)$ nonradiative transfer rate in the near-field region, I is the atomic nucleus spin, and $\{\ldots 6j\ldots\}$ is the well known $6j$ symbol. The effective nonradiative transfer rate between $|J_{\mathrm{e}}>$ and $|J_{\mathrm{g}}>$ states for atoms located in the near-field region is given by

$$\bar{A}^{f}_{J_{\mathrm{e}}\to J_{\mathrm{g}}} = \sum_{F_{\mathrm{e}}}\sum_{F_{\mathrm{g}}}\bar{A}^{f}_{F_{\mathrm{e}}\to F_{\mathrm{g}}} = A_{J_{\mathrm{e}}\to J_{\mathrm{g}}}\sum_{F_{\mathrm{e}}}\sum_{F_{\mathrm{g}}}\bar{\varepsilon}_{F_{\mathrm{g}}}\,g_{F_{\mathrm{e}}F_{\mathrm{g}}} \tag{11}$$

where $\bar{\varepsilon}_{F_{\mathrm{g}}}$ is the ratio between the nonradiative and radiative rates for the $6^2P_{3/2}\to 6^2S_{1/2}\left(F_{\mathrm{g}}\right)$ transition. Considering equations (5)–(7), one expects to have the 894 nm line profile similar to the one at 852 nm and different from the one at 455 nm. This is not the case regarding the experimental retrofluorescent spectral signals (Fig. 2). Even though mechanism (1) follows the linear dependence of intensity with respect to the laser power, it does not explain the spectra profiles at 894 nm. However, the experimental measurements exhibit similarities with 455 nm.

In the following subsection, we consider the other above-mentioned mechanism, having a contribution to the populating of the $6^2P_{1/2}$ level in the vapour irradiated by a laser tuned to the resonance 852 nm $\left(6^2S_{1/2}\to 6^2P_{3/2}\right)$ line.

4.2.2. Mechanism (2): collisions Cs (6^2D)+ Cs (6^2S)→ Cs (6^2P)+ Cs (6^2P)

The similarities between the experimental profiles of the 894 and 455 nm lines reasonably suggest considering a $6^2P_{1/2}$ populating process, with the participation of atoms excited by energy-pooling collisions, as a dominant contribution. Let us consider that the $6^2P_{1/2}$ level is populated starting from the 6^2D level and let us also consider reaction (2) as a dominant process; then, in the stationary regime, the population density of the $6^2P_{1/2}$ level would be given by (see Appendix A for details)

$$n_{6^2P_{1/2}}\left(x,\nu_{\mathrm{L}},F_{\mathrm{g}}\right) = \frac{k'_{6^2D\to 6^2P_{1/2}}\,n_{6^2S_{1/2}}}{\Gamma^{\mathrm{eff}}_{6^2P_{1/2}\to 6^2S_{1/2}}}\times n_{6^2D}\left(x,\nu_{\mathrm{L}},F_{\mathrm{g}}\right) \tag{12}$$

where

$$n_{6^2D}\left(x,\nu_{\mathrm{L}},F_{\mathrm{g}}\right) = \frac{1}{2}\,k^{(3/2)}_{6^2D}\,\tau^{\mathrm{eff}}_{6^2D}\,n^2_{6^2P_{3/2}}\left(x,\nu_{\mathrm{L}},F_{\mathrm{g}}\right) \tag{13}$$

and $\tau^{\mathrm{eff}}_{6^2D}$ is the effective lifetime of the 6^2D term in the gas. For qualitative illustration and comparison, by neglecting radiation-trapping effects in the vapour, the simplified form of the 894 nm line normalized retrofluorescence signal derived from mechanism (2) is given by

$$\phi_{894}(\nu_{\mathrm{L}},F_{\mathrm{g}}) \propto \frac{\bar{k}^{l}_{\mathrm{T}}(\nu_{\mathrm{L}})}{K''_0+2\bar{k}^{l}_{\mathrm{T}}(\nu_{\mathrm{L}})}\times F^2_{\nu_{\mathrm{L}}}\,\bar{k}^{l}_{\mathrm{T}}(\nu_{\mathrm{L}})\exp\left[-2\bar{\tau}^{f}_{\mathrm{T}}(\nu_{\mathrm{L}})\right] \tag{14}$$

Fig. 7. (*a*) Comparison between the measured and the calculated 894 nm ($6^2P_{1/2} \rightarrow 6^2S_{1/2}$) retrofluorescence signals for temperature $T = 106.3$ °C. (*b*) Theoretical curve based on mechanism (1) and (*c*) theoretical curve based on mechanism (2).

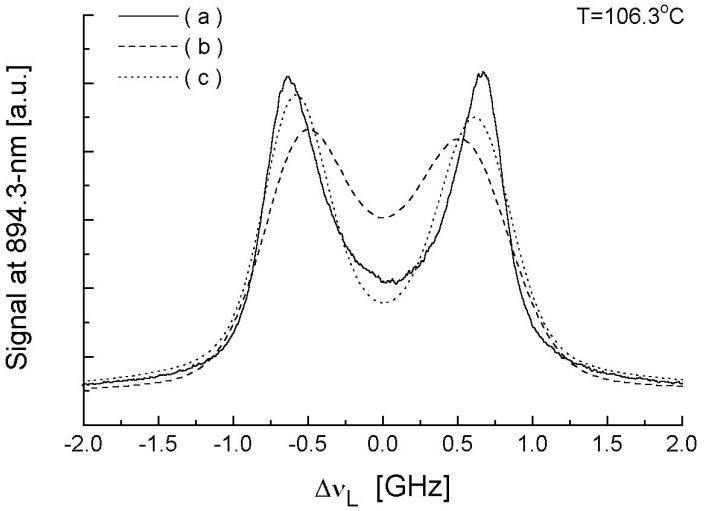

where K_0'' is a constant (for details see Appendix B).

One may note that the retrofluorescence signal, in the three cases, is principally determined by the coefficients $\bar{k}_{\mathrm{T}}^{l}(\nu_{\mathrm{L}})$ and $\bar{\tau}_{\mathrm{T}}^{f}(\nu_{\mathrm{L}})$ associated with the $6^2S_{1/2} \rightarrow 6^2P_{3/2}$ transition. The factor 2 appearing in the transfer filter for the 455 and 894 nm lines is due to the fact that $n_{7^2P_{3/2}}$ and $n_{6^2P_{1/2}} \propto n_{6^2P_{3/2}}^2$ (if mechanism 2 is considered dominant). Equation (14) shows that the signal at the 894 nm line is dominated by the term $\bar{k}_{\mathrm{T}}^{l}(\nu_{\mathrm{L}}) \exp\left[-2\bar{\tau}_{\mathrm{T}}^{f}(\nu_{\mathrm{L}})\right]$, which is the same as $\phi_{455}(\nu_{\mathrm{L}}, F_{\mathrm{g}})$. The multiplicative factor $\bar{k}_{\mathrm{T}}^{l}(\nu_{\mathrm{L}}) \big/ \left[K_0'' + 2\bar{k}_{\mathrm{T}}^{l}(\nu_{\mathrm{L}})\right]$ in (14) is a slowly varying term in the vicinity of zero detuning and is less than 1/2. Considering the expressions (5), (7), and (14), it is clear that we expect to have a retrofluorescence signal profile at 894 nm closer to the profile at 455 nm rather than to the profile at 852 nm. The theoretical difference between the signals at 894 and 455 nm is due to the factor $\bar{k}_{\mathrm{T}}^{l}(\nu_{\mathrm{L}}) / \left[K_0'' + 2\bar{k}_{\mathrm{T}}^{l}(\nu_{\mathrm{L}})\right]$; i.e, we have

$$\phi_{894}(\nu_{\mathrm{L}}, F_{\mathrm{g}}) \propto \phi_{455}(\nu_{\mathrm{L}}, F_{\mathrm{g}}) \times \frac{\bar{k}_{\mathrm{T}}^{l}(\nu_{\mathrm{L}})}{\left[K_0'' + 2\bar{k}_{\mathrm{T}}^{l}(\nu_{\mathrm{L}})\right]} \tag{15}$$

This factor may contribute to a slightly more pronounced dipping of the 894 nm profile compared with the 455 nm profile.

Let us consider the theoretical ratio $\eta_{\mathrm{tr}} = \phi_{894}/\phi_{852}$ between the 894 and 852 nm integrated retrofluorescence signals for the two mechanisms referred to here. From (5) and (6) derived from mechanism (1), the integrated retrofluorescence ratio is

$$\eta_{\mathrm{tr}} = \frac{\phi_{894}}{\phi_{852}} \propto \frac{K_0 + \bar{k}_{\mathrm{T}}^{l}(\nu_{\mathrm{L}})}{K_0' + \bar{k}_{\mathrm{T}}^{l}(\nu_{\mathrm{L}})} \tag{16}$$

This theoretical result is not in agreement with the observed value shown in Fig. 3. Now, considering mechanism (2), we have, from (5) and (14),

$$\eta_{\mathrm{tr}} \propto F_{\nu_{\mathrm{L}}} \bar{k}_{\mathrm{T}}^{l}(\nu_{\mathrm{L}}) \exp\left[-\bar{\tau}_{\mathrm{T}}^{f}(\nu_{\mathrm{L}})\right] \frac{K_0 + \bar{k}_{\mathrm{T}}^{l}(\nu_{\mathrm{L}})}{K_0'' + 2\bar{k}_{\mathrm{T}}^{l}(\nu_{\mathrm{L}})} \tag{17}$$

Contrary to (16), at a constant value of F_{ν_L}, relation (17) is compatible with the experimental result for the sensitized integrated retrofluorescence signal ratio.

A theoretical fit (*c*) of the experimental spectra (*a*), based on mechanism 2 for temperature $T = 106.3$ °C, is presented in Fig. 7. The calculation of the 894 nm retrofluorescence profile derived from mechanism 1 is also reported in Fig. 7*b*, for comparison with the experimental result. The computation has been carried out using the complete equation of the retrofluorescence signal given in Appendix B (B.3). The absorption shape of each component of the hyperfine structure $\alpha^{l,f}_{F_g \to F'_e}(\nu)$ (l for far-field and f for near field) is taken into account, F'_e being the quantum number of the hyperfine structure of the $6^2P_{1/2}$ level. The shapes of the absorption lines $\alpha^{l,f}_{F_g \to F'_e}(\nu)$ are of the Voigt type. The values of the atomic parameters (atomic line shapes $\alpha^{l,f}_{F_g \to F'_e}(\nu)$ FWHM and the effective ratio between the nonradiative and the radiative transfer rates $\bar{\varepsilon}'_{F_g}$ of the $\left(6^2P_{1/2} \to 6^2S_{1/2}\right)$ transition used in the calculation of the effective spectral absorption coefficient $\bar{k}^l_{F_g \to F'_e}(\nu)$ and the effective optical thickness $\bar{\tau}^f_{F_g \to F'_e}(\nu)$ were taken to be equal to those found for the $\left(6^2S_{1/2} \to 6^2P_{3/2}\right)$ transition in refs. 1 and 2. This numerical approximation has no significant effect on the profile of the calculated spectra because, as we are only concerned here with the laser frequency (ν_L) dependence of the retrofluorescence intensity, the theoretical normalized signal shape is mainly dominated by the optical coefficients $\bar{k}^l_T(\nu_L)$ and $\bar{\tau}^f_T(\nu_L)$ related to the laser frequency tuned to the $\left(6^2S_{1/2} - 6^2P_{3/2}\right)$ resonance. This approximation is also justified by the second mean value theorem applied to (B.3) in Appendix B. According to the theorem, an error in the exact values of $\alpha^{l,f}_{F_g \to F'_e}(\nu)$ and $\bar{\varepsilon}'_{F_g}$ will result in a modification of only the value of the constant K''_0 in (14), and the profile of the signal will be preserved. Choosing the same values as the $\left(6^2P_{3/2} \to 6^2S_{1/2}\right)$ transition is a reasonable numerical approximation. The other parameters for the computation are $\lambda' = 894.3$ nm, $J'_e = 1/2$, $J_g = 1/2$, $\bar{n}_{F_g}(T = 106.3\ °C) = 2.1 \times 10^{13}\text{cm}^{-3}$, and $A_{J'_e \to J_g} = 2.8 \times 10^7\ \text{s}^{-1}(J'_e)$ and J_g being the total angular momentum quantum number of $6^2P_{1/2}$ and $6^2S_{1/2}$ levels, respectively. There is fair agreement between the calculated profile (*c*) and the experimental signal (*a*). Mechanism (2) is compatible with the similarities between the experimental retrofluorescence profiles at 894 and 455 nm but does not predict the correct dependence of fluorescence intensity on the laser power. According to the model, the 894 nm retrofluorescence intensity may vary proportionally to the square of the laser intensity, at small power. An experimental check (not presented here) reveals a linear dependence of 894 nm line fluorescence intensity with respect to the incident laser power.

5. Conclusions

We have performed sensitized laser retrofluorescence spectroscopic experiments to investigate the signal associated with the 894 nm $\left(6^2P_{1/2} \to 6^2S_{1/2}\right)$ line in an optically thick cesium vapour excited by a weakly powered (between 20 and 570 μW for a beam area $\approx$0.014 cm^2), 10 MHz bandwidth diode laser tuned to the 852.2 nm $\left(6^2S_{1/2} \to 6^2P_{3/2}\right)$ resonance line. The cesium $\left[6^2S_{1/2}\left(F_g = 4\right) \to 6^2P_{3/2}\right.$ $\left.(F_e = 3, 4, 5)\right]$ hyperfine structures were selectively excited and the retrofluorescence signals associated with the $6^2P_{3/2}$ (852 nm), $6^2P_{1/2}$ (894 nm), and $7^2P_{3/2}$ (455 nm) levels have been measured. The experimental results reveal similarities between the 894 and 455 nm lines profiles and major differences between the 894 and 852 nm lines. Two populating mechanisms of the $6^2P_{1/2}$ level have been theoretically analyzed on the basis of the retrofluorescence model developed in refs. 1 and 2. Each one of the processes is compatible with only one characteristic aspect, as a function of the laser power or line shape of the experimentally obtained integrated retrofluorescence signals. We have pointed out that mechanism (1) gives the linear dependence of the retrofluorescence as a function of laser power but does not explain the spectrum profile, while mechanism (2) reproduces the 894 nm spectra profile but does not indicate the dependence of the retrofluorescence on laser power. There is an inconsistency between experimental and theoretical results that suggests that other mechanisms involving surface effects must

be taken into consideration to elucidate the line shapes of sensitized retrofluorescence near a dissipative surface. From the experimental observations, the collision number corresponding to process (1) cannot be estimated directly by the experimentally determined intensity ratios of both lines ϕ_{894} and ϕ_{852}, because the ratio is a function of the laser frequency. It would be interesting to complement this analysis with similar experiments in which the $6^2P_{1/2}$ level is optically pumped with a laser tuned to the 894 nm $\left(6^2S_{1/2} \rightarrow 6^2P_{1/2}\right)$ resonance line. Such measurements may provide quantitative information on the nonradiative de-excitation coefficient $\bar{A}^f_{6^2P_{1/2}\rightarrow 6^2S_{1/2}}$ of the $6^2P_{1/2}$ level near the dissipative surface of the glass cell. It would also be interesting to depopulate the 6^2D level, by using a second laser, and evaluate its effect on the retrofluorescence signal at 894 nm. It would also be useful to perform such experiments on other alkali metal vapours such as rubidium vapour.

Acknowledgments

This research was funded in part by the Natural Sciences and Engineering Research Council of Canada. We thank Oleg Volkov for helpful comments.

References

1. K. Le Bris, J.-M. Gagné, F. Babin, and M.-C. Gagné. J. Opt. Soc. Am. B, **18**, 1701 (2001).
2. J.-M. Gagné, K. Le Bris, and M.-C. Gagné. J. Opt. Soc. Am. B, **19**, 2852 (2002).
3. L. Krause. Appl. Opt. **5**, 1375 (1966).
4. A.N. Klyucharev and A.V. Lazarenko. Opt. Spectrosc. **32**, 576 (1972).
5. V.M. Borodin and I.V. Komarov. Opt. Spectrosc. **36**, 145 (1974).
6. Z.J. Jabbour, R.K. Namiotka, J. Huennekens, M. Allegrini, S. Milosevic, and F. de Tomasi. Phys. Rev. A, **54**, 1372 (1996).
7. C. Vadla, K. Niemax, and J. Brust. Z. Phys. D, **37**, 241 (1996); C. Vadla. Eur. Phys. J. D, **1**, 259 (1998).
8. F. de Tomasi, S. Milosevic, P. Verkerk, A. Fioretti, M. Allegrini, Z.J. Jabbour, and J. Huennekens. J. Phys. B: At. Mol. Opt. Phys. **30**, 4991 (1997).
9. R.R. Chance, A. Prock, and R. Silbey. J. Chem. Phys. **62**, 2245 (1975).
10. T. Yabuzaki, A.C. Tam, M. Hou, W. Happer, and S.M. Curry. Opt. Commun. **24**, 305 (1978).

Appendix A. Population density of the 6^2D and $6^2P_{1/2}$ atomic levels associated with mechanism (2)

To quantitatively treat the population densities of the 6^2D and $6^2P_{1/2}$ atomic levels, we make a number of approximations. We do not consider the fine-structure of the 6^2D $\left(=6^2D_{3/2+5/2}\right)$ atomic term. In our case, there is no (or very weak) radiative contribution to the population of 6^2D levels from higher lying levels. We also ignore the $6^2P_{3/2}+6^2P_{1/2}$ and $6^2P_{1/2}+6^2P_{1/2}$ collisional mixing when the monochromatic laser is tuned to the absorbing 852.2 nm $\left(6^2S_{1/2} \rightarrow 6^2P_{3/2}\right)$ line. We neglect the contributions of reaction (1) to the population of the $6^2P_{1/2}$ level in comparison to the contributions from the 6^2D level. The $\left(6^2D \rightarrow 6^2P_{1/2}\right)$ radiative contributions to the population of $6^2P_{1/2}$ are considered negligible compared with the collisional contribution $\left(6^2D+6^2S \rightarrow 6^2P+6^2P\right)$.

With these approximations, the rate equations for the 6^2D and $6^2P_{1/2}$ levels resulting from reaction (2) are

$$\frac{\mathrm{d}n_{6^2D}\left(x,\nu_{\mathrm{L}},F_{\mathrm{g}}\right)}{\mathrm{d}t}=k^{(3/2)}_{6^2D}\,\frac{n^2_{6^2P_{3/2}}\left(x,\nu_{\mathrm{L}},F_{\mathrm{g}}\right)}{2}-\frac{n_{6^2D}\left(x,\nu_{\mathrm{L}},F_{\mathrm{g}}\right)}{\tau^{\mathrm{eff}}_{6^2D}} \tag{A.1}$$

and

$$\frac{\mathrm{d}n_{6^2P_{1/2}}(x,\nu_\mathrm{L},F_\mathrm{g})}{\mathrm{d}t} = k'_{6^2D\to 6^2P_{1/2}}\, n_{6^2S_{1/2}}\, n_{6^2D}\left(x,\nu_\mathrm{L},F_\mathrm{g}\right) - \Gamma^{\mathrm{eff}}_{6^2P_{1/2}\to 6^2S_{1/2}}\, n_{6^2P_{1/2}}\left(x,\nu_\mathrm{L},F_\mathrm{g}\right) \quad \text{(A.2)}$$

where

$$\frac{1}{\tau^{\mathrm{eff}}_{6^2D}} = \left[\sum_J k'_{6^2D\to 6^2P_J} n_{6^2S_{1/2}} + \sum_J \Gamma^{\mathrm{eff}}_{6^2D\to 6^2P_J} + \sum_{J''} \Gamma^{\mathrm{eff}}_{6^2D\to 7^2P_{J''}}\right] \quad \text{(A.3)}$$

and $\tau^{\mathrm{eff}}_{6^2D}$ is the effective lifetime of the 6^2D level in the gas. $n_{6^2D}\left(x,\nu_\mathrm{L},F_\mathrm{g}\right)$ and $n_{6^2P_{1/2}}\left(x,\nu_\mathrm{L},F_\mathrm{g}\right)$ are, respectively, the population density of the 6^2D and $6^2P_{1/2}$ levels at position x when a laser of frequency ν_L selectively pumps the $6^2P_{3/2}$ state from the particular ground hyperfine level F_g. $\Gamma^{\mathrm{eff}}_{6^2D\to 7^2P_{J''}}$ is the effective radiative rate for the $\left(6^2D\to 7^2P_{J''}\right)$ transition; this coefficient appears in $\tau^{\mathrm{eff}}_{6^2D}$ as the radiative relaxation of the 6^2D level that also populates the 7^2P levels.

In the steady state regime, (A.1) and (A.2) have the solutions

$$n_{6^2D}\left(x,\nu_\mathrm{L},F_\mathrm{g}\right) = \frac{1}{2}\, k^{(3/2)}_{6^2D}\, \tau^{\mathrm{eff}}_{6^2D}\, n^2_{6^2P_{3/2}}\left(x,\nu_\mathrm{L},F_\mathrm{g}\right) \quad \text{(A.4)}$$

and

$$n_{6^2P_{1/2}}\left(x,\nu_\mathrm{L},F_\mathrm{g}\right) = \frac{k'_{6^2D\to 6^2P_{1/2}}\, n_{6^2S_{1/2}}}{\Gamma^{\mathrm{eff}}_{6^2P_{1/2}\to 6^2S_{1/2}}} \times n_{6^2D}\left(x,\nu_\mathrm{L},F_\mathrm{g}\right) \quad \text{(A.5)}$$

Using equation (9) from ref. 2

$$n_{6^2P_{3/2}}\left(x,\nu_\mathrm{L},F_\mathrm{g}\right) = \frac{F_{\nu_\mathrm{L}}}{h\nu_\mathrm{L}\Gamma^{\mathrm{eff}}_{6^2P_{3/2}\to 6^2S_{1/2}}}\, \bar{k}^l_\mathrm{T}(\nu_\mathrm{L}) \exp\left[-\bar{\tau}^f_\mathrm{T}(\nu_\mathrm{L})\right] \exp\left[-\bar{k}^l_\mathrm{T}(\nu_\mathrm{L})x\right] \quad \text{(A.6)}$$

where F_{ν_L} is the laser beam intensity at the cell entrance window, we have the following expression for the $6^2P_{1/2}$ population density:

$$n_{6^2P_{1/2}}(x,\nu_\mathrm{L},F_\mathrm{g}) = \frac{1}{2}\, \frac{F^2_{\nu_\mathrm{L}}}{\left(h\nu_\mathrm{L}\Gamma^{\mathrm{eff}}_{6^2P_{3/2}\to 6^2S_{1/2}}\right)^2}\, k^{(3/2)}_{6^2D} k'_{6^2D\to 6^2P_{1/2}}\, n_{6^2S_{1/2}}\, \tau^{\mathrm{eff}}_{6^2D} \times \left[\bar{k}^l_\mathrm{T}(\nu_\mathrm{L})\right]^2 \exp\left[-2\bar{\tau}^f_\mathrm{T}(\nu_\mathrm{L})\right] \exp\left[-2\bar{k}^l_\mathrm{T}(\nu_\mathrm{L})x\right] \quad \text{(A.7)}$$

Appendix B. Modelling of the 894 nm ($6^2P_{1/2} \to 6^2S_{1/2}$) retrofluorescence signal

The objective of this appendix is to present a simple model of the retrofluorescence signal produced by atoms excited in the $6^2P_{1/2}$ state due to mechanism (2). The procedure can be applied straightforwardly to the case of $6^2P_{1/2}$ populated by mechanism (1). Our modeling of the retrofluorescence signal takes into account the nonradiative phenomenon of photonic energy transformation near a dissipative surface. We also consider the hyperfine structures of the absorbing Cs $\left(6^2S_{1/2}\to 6^2P_{3/2}\right)$ transition and the Cs $\left(6^2P_{1/2}\leftrightarrow 6^2S_{1/2}\right)$ transitions. We use the physical and geometrical descriptions of the characteristic region of the cell schematically represented in Fig. B.1. The corresponding geometric

Fig. B.1. Backward radiance of a slice of vapour in a cell irradiated by a laser beam. Part of the incident laser energy is dissipated by the optical filter at the entrance. The fluorescent light emitted by the vapour of thickness dx located at distance x from the cell window passes through a filter of the same type when escaping the cell.

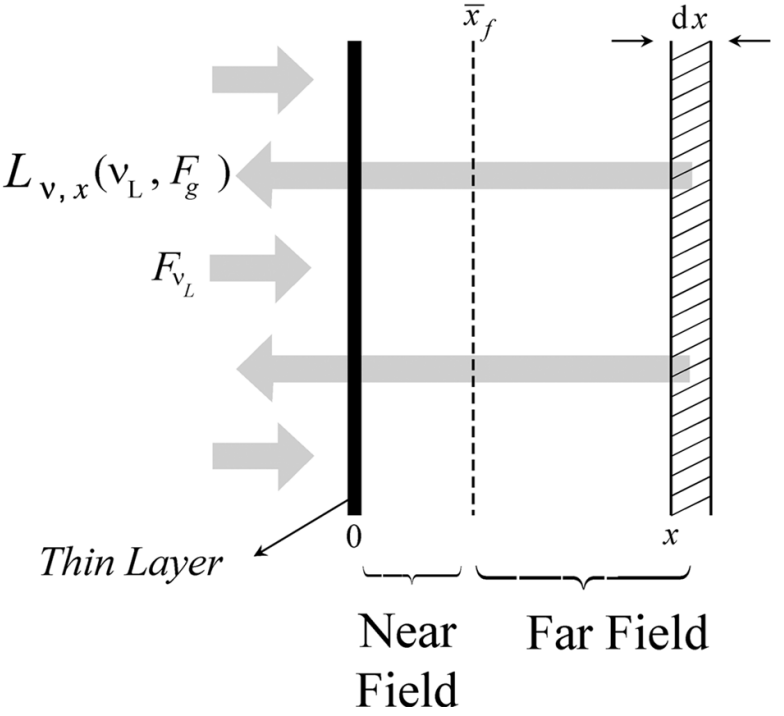

parameters are indicated. $\bar{x}_f$ is the mean geometrical depth of the near-field region ($\approx \lambda$). $L^{nl_J}(\nu_L, F_g)$ designates the integrated retrofluorescence radiance associated with the excited level (nl_J) evaluated at the origin $x = 0$ (at the entrance window) for a laser frequency ν_L, when the atoms are selectively pumped from the particular ground hyperfine level F_g. For simplification of the formulation, we neglect the reflection, absorption, and diffusion of the laser beam energy into the glass window and on the thin boundary layer on the glass.

The spectral radiance $L_{\nu,x}^{6^2P_{1/2}}(\nu_L, F_g)$ at $x = 0$, corresponding to the 894 nm $\left(6^2P_{1/2} \rightarrow 6^2S_{1/2}\right)$ transition, emitted by an elementary slab of vapour of thickness dx located at x (where only self-absorption processes are considered), is given by

$$L_{\nu,x}^{6^2P_{1/2}}\left(\nu_L, F_g\right) \propto \Gamma^{\text{eff}}_{6^2P_{1/2}\rightarrow 6^2S_{1/2}} \left(\sum_{F_g}\sum_{F'_e} g_{F'_e F_g} \alpha^{l}_{F'_e \rightarrow F_g}(\nu)\right) \exp\left[-\sum_{F_g}\sum_{F'_e} \bar{\tau}^{f}_{F_g \rightarrow F'_e}(\nu)\right] \times n_{6^2P_{1/2}}\left(x, \nu_L, F_g\right) \exp\left[-\sum_{F_g}\sum_{F'_e} \bar{k}^{l}_{F_g \rightarrow F'_e}(\nu)\, x\right] \quad \text{(B.1)}$$

where $\Gamma^{\text{eff}}_{6^2P_{1/2}\rightarrow 6^2S_{1/2}}$ is the effective radiative rate for the $\left(6^2P_{1/2} \rightarrow 6^2S_{1/2}\right)$ transition, $\bar{\tau}^{f}_{F_g \rightarrow F'_e}(\nu)$ is the effective optical spectral thickness of the stop-band filter at frequency ν, $\alpha^{l}_{F'_e \rightarrow F_g}(\nu)$ is the normalized emission profile in the far-field region and $\bar{k}^{l}_{F_g \rightarrow F'_e}(\nu)$ is the effective spectral absorption coefficient for the $\left[6^2S_{1/2}\left(F_g\right) \rightarrow 6^2P_{1/2}\left(F'_e\right)\right]$ transition line with F'_e, the quantum number of the

$6^2P_{1/2}$ level hyperfine structure ($F'_e = 3$ or 4). The coefficients $\bar{k}^l_{F_g \to F'_e}(\nu)$, $\bar{\tau}^f_{F_g \to F'_e}(\nu)$, and $g_{F'_e F_g}$ are given by relations identical to (8)–(10) on replacing the atomic parameters by those corresponding to the $6^2S_{1/2}(F_g) \to 6^2P_{1/2}(F'_e)$ transition. The 894 nm line signal $\phi_{894}(\nu_L, F_g)$ is proportional to the integrated radiance $L^{6^2P_{1/2}}(\nu_L, F_g)$ evaluated at $x = 0$

$$\phi_{894}(\nu_L, F_g) \propto L^{6^2P_{1/2}}(\nu_L, F_g) = \int_{\Delta\nu} \int_0^\infty L^{6^2P_{1/2}}_{\nu,x}\left(\nu_L, F_g\right)\, \mathrm{d}x\, \mathrm{d}\nu \tag{B.2}$$

Considering (A.7) and (B.1), (B.2) becomes

$$\phi_{894}(\nu_L, F_g) \propto F^2_{\nu_L}\left[\bar{k}^l_T(\nu_L)\right]^2 \exp\left[-2\bar{\tau}^f_T(\nu_L)\right] \times \int \frac{\bar{\alpha}^l_{894}(\nu)\exp\left[-\bar{\tau}^f_{894}(\nu)\right]}{\bar{k}^l_{894}(\nu) + 2\bar{k}^l_T(\nu_L)}\, \mathrm{d}\nu \tag{B.3}$$

where

$$\bar{\alpha}^l_{894}(\nu) = \sum_{F_g}\sum_{F'_e} g_{F'_e F_g}\, \alpha^l_{F'_e \to F_g}(\nu) \tag{B.4}$$

$$\bar{\tau}^f_{894}(\nu) = \sum_{F_g}\sum_{F'_e} \bar{\tau}^f_{F_g \to F'_e}(\nu) \tag{B.5}$$

and

$$\bar{k}^l_{894}(\nu) = \sum_{F_g}\sum_{F'_e} \bar{k}^l_{F_g \to F'_e}(\nu) \tag{B.6}$$

By applying the second mean value theorem for integrals to (B.3), the theoretical signal $\phi_{894}\left(\nu_L, F_g\right)$ takes the simpler form

$$\phi_{894}\left(\nu_L, F_g\right) \propto \frac{\bar{k}^l_T(\nu_L)}{K''_0 + 2\bar{k}^l_T(\nu_L)} \times F^2_{\nu_L}\, \bar{k}^l_T(\nu_L) \exp\left[-2\bar{\tau}^f_T(\nu_L)\right] \tag{B.7}$$

where K''_0 is a constant parameter associated with the mean value theorem.